

Exceptional cavity quantum electrodynamics

Yuwei Lu*

*School of Physics and Optoelectronics, South China University of Technology, Guangzhou 510641, China and
School of Physics and Optoelectronic Engineering, Foshan University, Foshan 528000, China*

Yanhui Zhao

School of Physics and Optoelectronic Engineering, Ludong University, Yantai 264000, China

Jingfeng Liu

College of Electronic Engineering, South China Agricultural University, Guangzhou 510642, China

An open quantum system operated at the spectral singularities where dimensionality reduces, known as exceptional points (EPs), demonstrates distinguishing behavior from the Hermitian counterpart. Based on the recently proposed microcavity with exceptional surface (ES), we report and explain the peculiar quantum dynamics in atom-photon interaction associated with EPs: cavity transparency, decoherence suppression beyond the limitation of Jaynes-Cummings (JC) system, and the population trapping of lossy cavity. An analytical description of the local density of states (LDOS) for the ES microcavity is derived from an equivalent cavity quantum electrodynamics (QED) model, which goes beyond the single-excitation approximation and allows exploring the quantum effects of EPs on multiphoton process by parametrizing the modified cascaded quantum master equation. It reveals that a square Lorentzian term in LDOS induced by second-order EPs interferes with the usual linear Lorentzian profile, giving rise to cavity transparency for atom with special transition frequency in the weak coupling regime. This additional contribution from EPs also breaks the limit on dissipation rate of JC system bounded by the bare components, resulting in the decoherence suppression with anomalously small decay rate of the long-time dynamics and the Rabi oscillation. Remarkably, we find that the cavity population can be partially trapped at EPs, achieved by forming a bound dressed state in the limiting case of vanishing atom decay. Our work unveils the exotic phenomena unique to EPs in cavity QED systems, which opens the door for controlling light-matter interaction at the quantum level through non-Hermiticity, and holds great potential in building high-performance quantum-optics devices.

I. INTRODUCTION

Exceptional points (EPs), the spectral degeneracies where two or more eigenvalues and the associated eigenstates simultaneously coalesce, are the central concept in non-Hermitian physics [1–5]. A plethora of intriguing effects and exotic phenomena emerge around EPs due to their nontrivial topological properties and the dimensionality reduction, including ultrasensitive sensing [6–11], laser mode selection [12, 13], chiral mode conversion [14–17], and unidirectional invisibility [18, 19]. Harnessing these peculiar features of non-Hermitian degeneracies for building novel devices with unprecedented performance has been experimentally demonstrated in various classical dissipative platforms, ranging from nanophotonics [2, 20–22], superconducting [23], cavity magnon polaritons [24–26], acoustics [27] to macroscopic facilities, such as fiber network [28], electric circuits [29] and heat diffusive system [30]. In recent years, great efforts have been dedicated to accessing the quantum EPs by implementing the non-Hermiticity in quantum systems [11, 24, 31–39], and investigating the quantum states control through EPs [17, 31–33, 38, 40–42]. In this respect, pioneer works have shown the ability of EPs to tune the photon statis-

tics [32, 33], enhance the sensitivity of quantum sensing [43, 44], and steer the evolution of single quantum system [17, 31, 38, 40–42, 45–47].

Despite these promising results, the quantum effects of EPs beyond wave mechanics is still largely unexplored. Recently, the emission properties of a quantum emitter (QE) in electromagnetic (EM) environments supporting EPs attracts growing attention [38, 40, 42, 45], since the modification of spontaneous emission (SE) features a squared Lorentzian profile around EPs, contrast to the nondegenerate resonances in conventional cavity with Lorentzian lineshape, and can lead to a greater enhancement of SE rate [40, 42, 45]. It implies that the formation of EPs in nanophotonic structures significantly alters the local density of states (LDOS), which fully describes the interaction between a QE and arbitrary EM environment [48–51]. Tailoring the LDOS of EM environment is crucial for optimizing the performance of many practical applications, ranging from traditional optoelectronic devices like lasers [52, 53] and solar cells [54], to advanced quantum technologies, such as quantum light sources [55–57] and logical gate [58, 59]. Therefore, a LDOS theory that can tackle the effects of EPs is of both fundamental and applied significance. The formalism of LDOS based on the classical Green function separates the EPs contribution from the usual Lorentzian term [40, 41, 60], while it leaves the origin of EPs unclear, i.e., information of

* Corresponding Author: luyw5@fosu.edu.cn

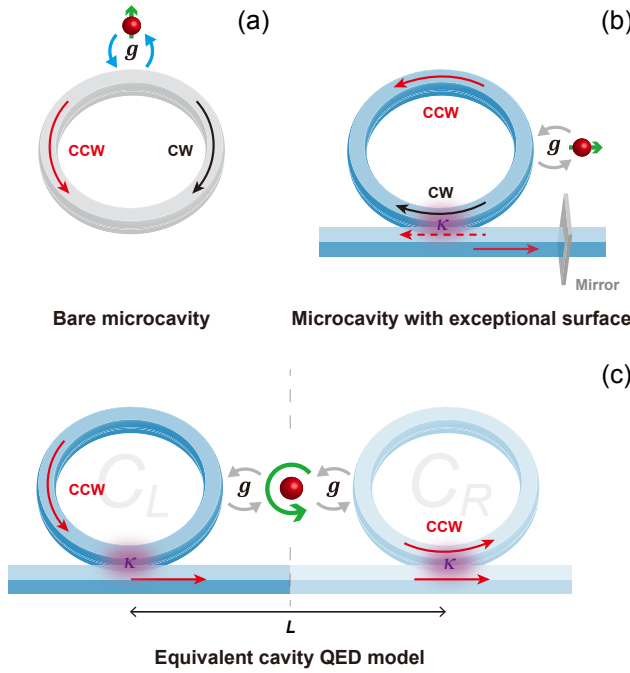


FIG. 1. Schematic diagrams of cavity QED model. (a) A whispering-gallery-mode (WGM) cavity represented by microring resonator supports the degenerate clockwise (CW) and counterclockwise (CCW) modes, and is operated at a diabolic point (DP). A linearly polarized quantum emitter (QE) is simultaneously coupled to both CW and CCW modes with equal coupling rate. (b) A microring cavity coupled to a semi-infinite waveguide with a mirror at the one side can create an exceptional surface due to the chiral coupling between CW and CCW modes. (c) Conceptual illustration of the equivalent cavity QED model for the system in (b) with a perfect mirror, where the CW mode is flipped to another CCW mode through mirror symmetry, and the linearly polarized QE is replaced by a circularly polarized one. The distance between the original and the mirrored cavities is L .

the underlying cavity resonances is ambiguous, the parameters of coalescent cavity modes that forms EPs are implicit, and thus the EPs condition cannot be given explicitly. As a consequence, there are at least two obvious limitations that hinder the exploration of quantum effects of EPs using macroscopic QED based on the classical Green function: the quick and accurate design of nanophotonic structures that possess EPs remains challenging, and the nonlinear regime of cavity QED involving multiphoton interaction is exclusive.

To overcome the aforementioned limitations of current LDOS theory for EPs, in this work we propose an equivalent cavity QED model that can provide an intuitive and flexible quantum master equation (QME) approach for a class of novel microcavity with exceptional surface (ES) [8, 11, 61–63], also known as chiral EPs. An analytical description of LDOS for such ES microcavity is derived, and parametrized by the resonance frequencies, decay rates and dissipative coupling rate of discrete cavity modes, as well as the coupling rates between the cavity modes and

the QE. Therefore, it establishes an explicit connection with the quantum dynamics at EPs. Furthermore, the formulation of SE spectrum is also obtained to unveil the peculiar quantum dynamics at EPs. Our LDOS theory not only explains the exotic properties of SE dynamics related to EPs previously known only with the special parameters choice [41, 42], but also allows the entire formalization, and thus provides insight into the effects of EPs in open quantum systems.

The rest of paper is organized as follows. In Sec. II, we describe our equivalent cascaded cavity QED model of ES microcavity. The corresponding equations of motion, LDOS, and the SE spectrum are derived from the QME. Sec. III presents some peculiar features of quantum dynamics at EPs, and explains from the LDOS and the SE spectrum. We conclude in Sec. IV.

II. MODEL AND THEORY

Different strategies have been proposed to construct an ES in whispering-gallery-mode (WGM) cavity, by introducing the additional scattering structures [8, 63] or coupling to a waveguide terminated by a mirror at the one side [11, 42]. The cavity QED model for the former can be developed by treating the scattering structures as Rayleigh-type nanoparticles [63, 64], while the latter should be considered as a cascaded system [65, 66] instead in the framework of waveguide QED [67–69] due to the existence of mirror. The formation of ES, a collection of EPs in a high-dimensional parameter space rather a single EP, results from the unidirectional coupling between the clockwise (CW) and the counterclockwise (CCW) modes assisted by the auxiliary reservoir modes. Therefore, the underlying physical mechanism is similar for two implementations. Here we employ the latter scheme for the sake of theoretical simplicity, but the results and conclusions presented in this work are suitable for other type of ES microcavity.

Fig. 1(a) depicts a basic cavity QED system consisting of a WGM microcavity and a quantum emitter (QE). The QE is linearly polarized, and coupled to a pair of degenerate CW and CCW modes with equal coupling rate g . Since there is no interaction between two cavity modes, the system is operated at a diabolic point (DP) and described by the Jaynes-Cummings (JC) model. By coupling the WGM microcavity to a semi-infinite waveguide with a mirror at the right end, a unidirectional coupling from CCW mode to CW mode is created, as Fig. 1(b) illustrates. This photonics structure exhibits a surface of second-order EPs in parameter space, and offers great tunability to SE rate of a QE. In order to develop an intuitive cavity QED model for this novel ES microcavity, we transform the system to an equivalent one through mirror symmetry, as shown in Fig. 1(c). The original CW mode is flipped to a mirrored CCW mode, and the corresponding left-handed emission of QE is converted to the right-handed emission into the mirrored CCW mode

as well. As a result, the linearly polarized QE becomes circularly polarized in the equivalent cavity QED model. Two cavities in the equivalent model constitutes a cascaded system [65, 66, 70], the quantum dynamics is described by the modified cascaded QME ($\hbar = 1$)

$$\begin{aligned} \dot{\rho} = & -i[H_0 + H_I, \rho] + \gamma\mathcal{L}[\sigma_-]\rho + \kappa\mathcal{L}[c_L]\rho + \kappa\mathcal{L}[c_R] \\ & + \kappa|r|\left(e^{i\varphi}\left[c_L\rho, c_R^\dagger\right] + e^{-i\varphi}\left[c_R, \rho c_L^\dagger\right]\right) \end{aligned} \quad (1)$$

where $\mathcal{L}[O]\rho = O\rho O^\dagger - \{O^\dagger O, \rho\}/2$ is the Liouvillian superoperator. The second line of Eq. (1) describes the unidirectional coupling from CCW mode to CW mode, where $|r|$ is the reflectivity of mirror, and $\phi = \beta L$ is the phase factor, with β and L being the propagation constant of waveguide and the distance between two cavities, respectively. The free Hamiltonian H_0 and the interaction Hamiltonian H_I are given by

$$\begin{aligned} H_0 &= \omega_0\sigma_+ + \omega_c c_L^\dagger c_L + \omega_c c_R^\dagger c_R \\ H_I &= g\left(e^{-i\phi}c_L^\dagger\sigma_- + h.c.\right) + g\left(e^{i\phi}c_R^\dagger\sigma_- + h.c.\right) \end{aligned} \quad (2)$$

where σ_- is the lowering operator of QE with transition frequency ω_0 and SE rate γ in homogeneous medium. c_L and c_R are the bosonic annihilation operators for CCW modes of the original and mirrored microcavities with resonance frequency ω_c , respectively. κ is the dissipative coupling rate between the cavity modes and the waveguide. The intrinsic decay of two CCW modes is omitted, considering that the evanescent coupling to waveguide dominating the cavity dissipation. The phase factor ϕ originates from the traveling wave nature of WGM modes and depends on the azimuthal orientation of QE location [71, 72]. From Eq. (1), we take the operator expectation values to obtain the equations of motion

$$\frac{d}{dt}\vec{p} = -i\mathbf{M}\vec{p} \quad (3)$$

where $\vec{p} = (\langle c_L \rangle, \langle c_R \rangle, \langle \sigma_- \rangle)^T$ and the 3×3 matrix takes the form

$$\mathbf{M} = \begin{pmatrix} \omega_c - i\frac{\kappa}{2} & 0 & ge^{-i\phi} \\ -i\kappa|r|e^{i\varphi} & \omega_c - i\frac{\kappa}{2} & ge^{i\phi} \\ ge^{i\phi} & ge^{-i\phi} & \omega_0 - i\frac{\gamma}{2} \end{pmatrix} \quad (4)$$

The normalized LDOS, i.e., Purcell factor, is expressed as $P(\omega) = 2\pi J(\omega)/\gamma$, where $J(\omega) = \int_{-\infty}^{+\infty} d\tau e^{i\omega\tau} g^2 \left\langle \left[c_L^\dagger(0) + e^{-i2\phi}c_R^\dagger(0)\right] \left[c_L(\tau) + e^{i2\phi}c_R(\tau)\right] \right\rangle$ is the spectral density of ES microcavity. The correlation functions can be calculated by applying the quantum regression theorem $\langle O_i O_j(\tau) \rangle = \sum_k M_{jk}(\tau) \langle O_i O_j \rangle$ [73] with the following QME

$$\begin{aligned} \dot{\rho} = & -i[H_0, \rho] + \kappa\mathcal{L}[c_L]\rho + \kappa\mathcal{L}[c_R]\rho \\ & + \kappa|r|\left(e^{i\varphi}\left[c_L\rho, c_R^\dagger\right] + e^{-i\varphi}\left[c_R, \rho c_L^\dagger\right]\right) \end{aligned} \quad (5)$$

since the initial state of EM environment is the vacuum state. We arrive at

$$J(\omega) = -g^2 \text{Im}[2\chi_{\text{DP}}(\omega) + \chi_{\text{EP}}(\omega)] \quad (6)$$

with the usual linear Lorentzian response, i.e., DP term

$$\chi_{\text{DP}}(\omega) = \frac{1}{(\omega - \omega_c) + i\kappa/2} \quad (7)$$

and the additional EP contribution

$$\chi_{\text{EP}}(\omega) = \frac{-i\kappa|r|e^{i\Delta\phi}}{[(\omega - \omega_c) + i\kappa/2]^2} \quad (8)$$

where $\Delta = \varphi - 2\phi$ is the phase difference. The factor 2 of $\chi_{\text{DP}}(\omega)$ represent that the QE is coupled to two cavity modes. Eq. (8) clearly indicates the squared Lorentzian profile of $\chi_{\text{EP}}(\omega)$, a signature of second-order EPs. However, it also indicates that any loss of reflection amplitude, i.e., an imperfect mirror with $|r| < 1$, will degrade the quantum effects of EPs. In the following study, we take $|r| = 1$ unless specially noted. We highlight that our approach can also be applied to a more general case where the coupling between two cavities are bidirectional but asymmetrical, for example, introducing a Rayleigh scatter in close proximity of microring [8, 19, 64]. As a result, the system is drawn out of ES, and such configuration can be utilized to study the emergence of quantum effects of EPs. Furthermore, one can obtain the LDOS of target nanophotonic structure that owns desirable quantum effects of EPs for EM design. This is important for nanophotonic structure optimization, especially for these consisting of absorbing and dispersing medium like plasmonic-photonic cavity [74–77], where the coupling constant between cavity modes is hard to evaluate, contract to the ES microcavity studied in this work. On the other hand, the quantum-optics properties of a given nanophotonic structure are predictable, by parametrizing the modified cascaded QME (Eq. (1)) using the simple curve fitting of LDOS obtained from EM simulations. Therefore, Eqs. (7) and (8) build the bridge between the EM design of nanophotonic structures and the quantum state control by EPs.

The exotic quantum dynamics at EPs can be understood from the spectral properties of QE. The emission spectrum of QE is defined as $S(\omega) = (2\pi)^{-1} \int_0^\infty dt_2 \int_0^\infty dt_1 e^{-i\omega(t_2-t_1)} \langle \mathbf{E}^-(\mathbf{r}, t_2) \cdot \mathbf{E}^+(\mathbf{r}, t_1) \rangle$ [73], with $\mathbf{E}^-(\mathbf{r}, t_1) = [\mathbf{E}^+(\mathbf{r}, t_1)]^\dagger$ and $\mathbf{E}^+(\mathbf{r}, t) = e^{-i\omega_0 t} \int_0^t dt' \mathbf{G}(t, t') \sigma_-(t') e^{i\omega_0 t'}$, where $\mathbf{G}(t, t')$ is a kind of propagator. For assuming an initially excited QE and $\mathbf{r} = \mathbf{r}_0$, where \mathbf{r}_0 is the QE position, $S(\omega)$ becomes the SE spectrum, also called the dipole spectrum [78, 79], which reflects the local dynamics of a QE, and can be analytically expressed as

$$S(\omega) = \frac{1}{\pi} \frac{\gamma + \Gamma(\omega)}{[\omega - \omega_0 - \Delta(\omega)]^2 + \left[\frac{\gamma + \Gamma(\omega)}{2}\right]^2} \quad (9)$$

with the photon induced Lamb shift

$$\Delta(\omega) = g^2 \text{Re}[2\chi_{\text{DP}}(\omega) + \chi_{\text{EP}}(\omega)] \quad (10)$$

and the local coupling strength

$$\Gamma(\omega) = -2g^2 \text{Im}[2\chi_{\text{DP}}(\omega) + \chi_{\text{EP}}(\omega)] \quad (11)$$

Note that the SE dynamics of QE can be retrieved from $\mathcal{F}[S(\omega)]$, the Fourier transform of SE spectrum $S(\omega)$. Eqs. (9)-(11) indicates that LDOS is crucial for understanding the exotic behavior of quantum dynamics at EPs. The contributions of DP and EP are separated in Eqs. (10) and (11), which is beneficial to unravel how the emergence of EPs alters the quantum dynamics.

III. RESULTS AND DISCUSSION

A. Cavity transparency

We first consider the weak coupling regime, where the Purcell effect is expected to modify the SE rate of a QE. Note that the quality factor of modes in ES microcavity is typically 10^4 due to the dissipative coupling to external structures, therefore, we will focus on the case for $\kappa \gg \gamma$ in the following discussion. Fig. 2(a) shows the SE dynamics for QEs with different γ , while the coupling rate g and the cooperativity $C = 8g^2/\kappa\gamma = 0.2$ are set to be fixed. With resonant QE-cavity coupling, the Purcell factor is equal to the cooperativity C , and thus QEs in DP cavity experience the Purcell enhancement and the corresponding SE dynamics manifests a faster decay, as shown by the dashed lines in Fig. 2(a). On the contrary, the SE dynamics of QEs in ES cavity is counterintuitive, which shows good accordance with QEs in the free space as if the cavity is absent. Therefore, we call this intriguing phenomenon as cavity transparency. The same effect has been reported in Ref. [42] and explained as a consequence of decoupling between the QE and the cavity modes due to the special electric field pattern forming at EPs. Here, we unravel from the perspective of LDOS that the cavity transparency in ES microcavity results from the precise cancellation of EP and DP contributions at special frequency point, giving arise to null Purcell factor for a QE with the same transition frequency.

The zero point of Purcell factor can be found from Eqs. (6)-(8) by letting $J(\omega) = 0$, the solution takes a simple form

$$\Delta\omega = \Delta\omega_m \equiv -\frac{\kappa}{2} \tan\left(\frac{\Delta\phi}{2}\right) \quad (12)$$

where $\Delta\omega = \omega - \omega_c$ is the frequency detuning. Fig. 2(b) displays the LDOS versus $\Delta\omega$ and $\Delta\phi$, which can be easily tuned by varying the mirror location, i.e., the waveguide length L . We can see that the zero point of LDOS goes away from cavity resonance as $\Delta\phi$ increase from 0 to π , and the opposite tendency is observed for $\Delta\phi \in [\pi, 2\pi]$, while the frequency of zero point is larger than cavity resonance in this case. Especially, the null Purcell factor is achieved at the cavity resonance with $\Delta\phi = 0$, which is just the circumstance studied in Ref. [39]. Fig. 2(c) plots the decomposition of LDOS for $\Delta\phi = 0$ and $\pi/2$, where we reverse the EP term by taking a negative sign to display the cancellation of EP and DP contributions. It shows that the EP term can be negative and weaken

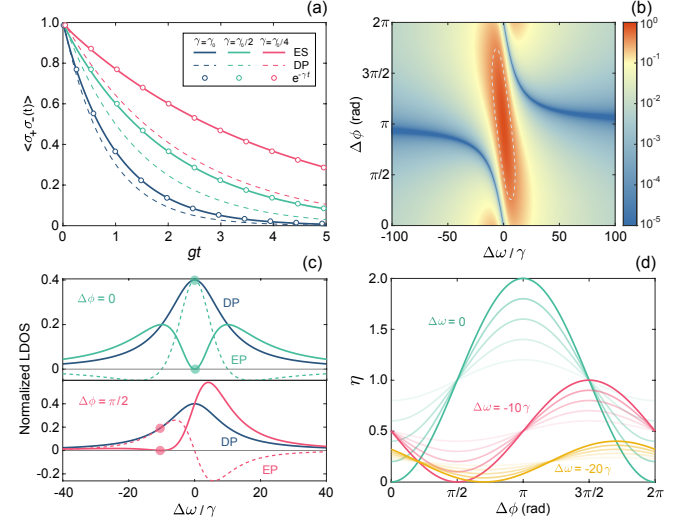


FIG. 2. Cavity transparency and LDOS of ES microcavity. (a) Comparison of the spontaneous emission dynamics of a QE resonantly and weakly coupled to the ES (solid lines) and DP (dashed lines) microcavities with different decay rates γ . The QE dynamics in the free space is also shown. The parameters are $g = \gamma_0$ and $g^2/\kappa\gamma = 1/40$, where γ_0 is the unit rate of atom decay. (b) LDOS of ES microcavity versus frequency and phase difference $\Delta\phi$, with $g = \gamma$ and $\kappa = 20\gamma$. The gray dashed line indicates the parameter region for Purcell factor enhancement $\eta > 1$. (c) Decomposition of LDOS of ES microcavity versus frequency for $\Delta\phi = 0$ and $\pi/2$. The DP and EP contributions are plotted by the solid blue lines and the dashed color lines, respectively. (d) η of ES microcavity as the function of phase difference for various $\Delta\omega$. $|r|$ declines from 1.0 to 0.2 in a linear fashion for curves with the same color from dark to light. The parameters of (c) and (d) are the same as (b).

the Purcell effect. For $\Delta\phi = 0$, the EP response features an even symmetry and a narrow profile. The resultant LDOS is slightly enhanced at a wide frequency range far detuned from the cavity, but strongly suppressed around the cavity resonance. The EP response cancels the DP contribution at cavity resonance, and results in the vanishing Purcell enhancement for a QE resonantly coupled to the ES microcavity. The lower panel of Fig. 2(c) shows that the EP response exhibits a totally different profile for $\Delta\phi = \pi/2$, which becomes odd symmetry and changes its sign at cavity resonance. As a result, the disappear Purcell effect occurs at the left side of cavity resonance ($\Delta\omega_m < 0$), while the enhanced Purcell effect is observed at the whole frequency range of $\omega > \omega_c$, leading to a strongly asymmetrical LDOS.

Fig. 2(d) plots the Purcell factor enhancement of EPs as the function of $\Delta\phi$ for various $\Delta\omega$ and $|r|$, which is defined as $\eta = P(\omega)/C$. It shows that EPs attain greatest tunability to Purcell effect at resonant QE-cavity coupling, where a double increase of Purcell factor compared to a DP cavity can be realized with a perfect mirror and $\Delta\phi = \pi$, and thus permit the stronger light-matter in-

teraction. Detuned from the cavity resonance, the null Purcell factor still exists with $|r| = 1$, but the maximum η decreases. $\eta > 1$ can be achieved inside the parameter region indicated by the gray dashed line in Fig. 2(b). Fig. 2(d) also shows that the maximum η drops as the loss of reflection amplitude increases, but a mirror with $|r| > 0.8$ still holds great tunability of Purcell effect. It is worth noting that $|r| \sim 0.97$ is achievable [42, 56], and thus a practical mirror will not significantly weaken the ability of EPs to tune the Purcell effect in experiment.

B. Anomalous decay and population trapping

The above analysis reveals that EPs have the ability to significantly modify the SE process, from completely suppressed to enhanced Purcell effect, and thus the ES microcavity can provide greater degrees of freedom to control the light-matter interaction than a DP cavity. We now go beyond the weak coupling regime and study the long-time dynamics of QE decaying in ES microcavity, where the eigenenergy with minimum decay (ω_m) dominates the system evolution. In a DP cavity, the decoherence always takes place with a rate greater than γ for $\kappa \gg \gamma$. For the ES microcavity, the minimum decoherence rate can be obtained by finding an optimal QE-cavity detuning ($\Delta\omega_{\text{opt}}$) for achieving a smallest decay of ω_m , denoted as $\Gamma = -\text{Im}[\omega_m]$. From the denominator of SE spectrum (Eq. (9)), we obtain

$$\Delta\omega_{\text{opt}} = \frac{2g^2}{\kappa} \sin(\Delta\phi) + \Delta\omega_m \quad (13)$$

where the limitation $\gamma \rightarrow 0$ has been taken. We can see that Eq. (13) encompasses the case of cavity transparency, with $g \ll \kappa$ in the weak coupling regime. As g increases, the contribution of the first term in Eq. (13) becomes significant, the resultant $\Delta\omega_{\text{opt}}$ is no longer overlapped with the location of null Purcell factor for $\Delta\phi \neq 0$. As shown by Fig. 3(a), the greatest deviation occurs around $\Delta\phi = \pi/2$. Fig. 3(b) plots the minimum decoherence rate Γ corresponding to $\Delta\omega_{\text{opt}}$ for various g , where we can see that the decoherence rate reaches the minimum at $\Delta\phi = 0$, and increases as $\Delta\phi$ varies from 0 to π . Remarkably, the decoherence rate in ES microcavity can be smaller than $\gamma/2$, which is below the limit of JC system for $\kappa \gg \gamma$, and thus is not possible for a DP cavity. We can also see that enhancing the QE-cavity interaction is beneficial to reduce the decoherence rate, and a tenfold reduction ($\Gamma \approx \gamma/20$) can be achieved with a moderate QE-cavity coupling $g = 20\gamma$ at $\Delta\phi = 0$. While for any value of g , $\Gamma \rightarrow \gamma/2$ as $\Delta\phi$ approaches to π , it implies that the minimum decoherence rate at $\Delta\phi = \pi$ is achieved by decoupling the QE from the cavity.

Fig. 3(c) compares the long-time dynamics of initial excited QEs in the free space and in ES microcavity with optimal detuning $\Delta\omega_{\text{opt}}$ from the cavity. We can see from the slope of decay curves that the EPs can offer different

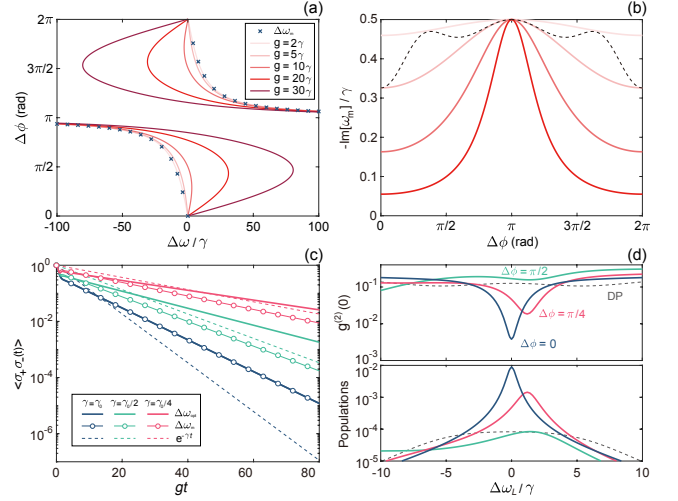


FIG. 3. Anomalous decay in ES microcavity. (a) Comparison of the location of zero LDOS $\Delta\omega_m$ and the optimal atom-cavity detuning $\Delta\omega_{\text{opt}}$ corresponding to the minimum decay of eigenenergy level Γ in the single-excitation subspace for various g . (b) Γ as the function of $\Delta\phi$ for various g . $\Delta\omega_m$ for $g = 5\gamma$ (black dashed line) is shown for comparison. In (a) and (b), $\kappa = 20\gamma$. (c) Logarithmic plot of QE dynamics with detuning $\Delta\omega_{\text{opt}}$ (solid lines) and $\Delta\omega_m$ (thin solid lines with circle) from cavity for various $\Delta\phi$. The parameters are $g = 5\gamma$ and $g^2/\kappa\gamma = 5/4$, where γ_0 is the unit rate of atom decay. Note that the SE rate γ is taken to be γ_0 , $\gamma_0/2$, and $\gamma_0/4$ for $\Delta\phi = 0$, $\pi/4$, and $\pi/2$, respectively, to distinguish different curves, but the corresponding Γ is still the curve of $g = 5\gamma$ in (b). The dynamics of bare QEs is shown for comparison (dashed lines). (d) $g^{(2)}(0)$ (upper panel) and population (lower panel) of c_L cavity as the function of frequency in the case of c_R cavity drive. The results are numerically calculated by implementing a driving Hamiltonian $H_d = \Omega (c_R^\dagger + c_R)$ in the modified cascaded QME (Eq. (1)) and using QuTip [80], with parameters $g = 5\gamma$, $\kappa = 20\gamma$, $\Delta\phi = 0$, $\Delta_{0c} = \Delta\omega_{\text{opt}}$, and driving strength $\Omega = 0.2\gamma$.

degrees of suppression on the decoherence process, according to the value of $\Delta\phi$. As a result, the population of QEs in ES microcavity can be larger than the bare QEs for $t > 50g^{-1}$, as well as the QEs in ES microcavity but with detuning $\Delta\omega_m$ for $\Delta\phi \neq 0$. The corresponding Γ for QEs with detuning $\Delta\omega_m$ is plotted as the dashed black line in Fig. 3(b). It shows that though smaller than $\gamma/2$, Γ of QEs with detuning $\Delta\omega_m$ evidently increases at both $\Delta\phi = \pi/4$ and $\pi/2$ compared to that of QEs with optimal detuning $\Delta\omega_{\text{opt}}$ (curve of $g = 5\gamma$). Therefore, the resultant population is even lower than a bare QE for $t > 100g^{-1}$, due to the fast depletion by cavity at the initial stage of decay.

The significantly reduced decay of eigenenergy makes the ES microcavity-QE system advantageous for single-photon generation exploiting the photon blockade [81, 82], where the photon antibunching takes place at the energy of eigenenergy levels in the single-excitation subspace with a coherent input. Therefore, single-photon

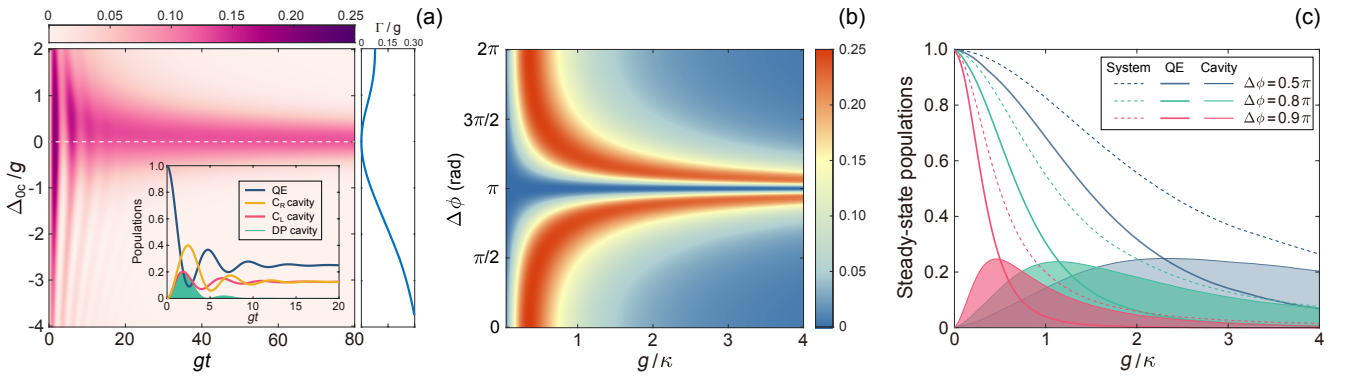


FIG. 4. Population trapping of ES microcavity with vanishing atom decay. (a) Time dynamics of cavities population as the function of QE-cavity detuning Δ_{0c} , with parameters $\Delta\phi = \pi/2$ and $g = 10\gamma$. The inset shows the time dynamics at $\Delta_{0c} = 0$. The right panel plots Γ as the function of Δ_{0c} . (b) Steady-state cavity population versus g and Δ_{0c} . (c) Steady-state populations of QE (solid lines), cavities (thin solid lines with shading), and their sum (dashed lines) as the function of g for various $\Delta\phi$. In all figures, $\kappa = 20\gamma$.

blockade can attain efficiency improvement by utilizing the ES microcavity. In the CW mode (c_R) driven case, Fig. 3(d) compares the single-photon purity $g^{(2)}(0) = \langle c_X^\dagger c_X^\dagger c_X c_X \rangle / n_X^2$ and population $n_X = \langle c_X^\dagger c_X \rangle$ of DP and ES microcavities, with $X = R, L$, and parameters $\Delta\phi = 0$, $g = 5\gamma$ and $\kappa = 20\gamma$. We evaluate $g \approx g_c = \sqrt{(\kappa^2 + \gamma^2)/4}$, where g_c is the critical coupling rate of strong coupling for a DP cavity [83]. It implies that the strong antibunching is absent in DP cavity, since the system just reaches the strong coupling regime. As shown in Fig. 3(d), $g^{(2)}(0)$ curve of DP cavity is flat, and the minimum $g^{(2)}(0)$ is ~ 0.1 . With the resonant QE-cavity coupling, which is also the optimal configuration detuning according to Eq. (13), the CCW mode of ES microcavity (c_L) demonstrates a great enhancement of single-photon purity by over an order of magnitude at $\Delta\phi = 0$, with the minimal $g^{(2)}(0) \sim 0.005$, accompanied by a hundredfold improvement of population. While for $\Delta\phi = \pi/4$, the single-photon purity and population are both improved by about an order of magnitude in ES microcavity. Therefore, ES microcavity shows great potential in building high-efficiency single-photon source.

Inspired by the results of Fig. 3(c) that the long-time decay rate of a QE can be smaller than its SE rate in the free space, we then consider a limiting case of $\gamma \rightarrow 0$. The eigenenergy corresponding to $\Delta\omega_{\text{opt}}$ is found as $\omega_m = \Delta\omega_m$, which is purely real in this case, signifying the formation of an atom-photon bound state at EPs, except for $\Delta\phi = \pi$, where the QE is decoupled from the cavity and remains in the excited state. The physical mechanism of atom-photon bound state at EPs is similar to the accidental bound states in the continuum (BIC) [84–86], also known as Friedrich-Wintgen BIC, which results from the destructive interference of two coupling pathways between cavities, the direct coupling and the indirect coupling mediated by dissipative channel. While in ES microcavity, the difference is that the direct cou-

pling is replaced by the QE-mediated coupling, and the dissipation-mediated coupling is unidirectional.

Fig. 4(a) shows the time evolution of cavities population versus QE-cavity detuning $\Delta_{0c} = \omega_0 - \omega_c$, with parameters $\Delta\phi = \pi/2$, $g = 10\gamma$, and $\kappa = 20\gamma$. Eq. (13), as well as Γ , indicate that the bound state achieved at $\Delta_{0c} = 0$, see the blue line in the right panel of Fig. 4(a). As a result, the decay of cavity population is obviously slower around $\Delta_{0c} = 0$, and the populations of QE and two CCW modes are partially trapped after a few cycles of Rabi oscillation at $\Delta_{0c} = 0$, as shown by the inset of Fig. 4(a). It shows that though the steady-state populations of two cavities are the same, c_R cavity exhibits stronger Rabi oscillation due to the unidirectional energy transfer from c_L cavity. The maximum population of c_R cavity reaches 0.4, while that of c_L cavity is about 0.2. By contrast, the population trapping cannot be realized in a DP cavity without the bound state, as shown by the green line with shading.

Fig. 4(b) displays the steady-state cavities population versus $\Delta\phi$ and g . It reveals that for a given $\Delta\phi$, there is an optimal g for maximum population, denoted as $P_c^{\text{opt}}(\Delta\phi)$, which is maximal at $\Delta\phi = 0$, i.e., $P_c^{\text{opt}}(0)$ is the upper bound of steady-state cavities population. $P_c^{\text{opt}}(\Delta\phi)$ is evaluated to decrease by 0.03 as $\Delta\phi$ varies from 0 to 0.9π , and thus is robust against the variation of $\Delta\phi$. For $\Delta\phi = 0$, the steady-state populations can be analytically given from Eq. (3), which are $P_e^{\text{ss}} = \kappa^4 / (8g^2 + \kappa^2)^2$ for QE and $P_c^{\text{ss}} = 8g^2\kappa^2 / (8g^2 + \kappa^2)^2$ for cavities. We can see that P_e^{ss} reduces as g increase, exhibiting distinguishing feature from P_c^{ss} . Furthermore, we can obtain $P_c^{\text{opt}}(0) = 0.25$, and the expression of leaky energy $P_\kappa^{\text{ss}} = 8g^2 / (8g^2 + \kappa^2)$, which is monotonically increasing with respect to g . It implies that the optimal g for maximum cavities population is the result of balance between the population transfer from QE and the system dissipation. Fig. 4(c) plots the steady-state populations versus g for various $\Delta\phi$. It shows that for $\Delta\phi > 0.9\pi$,

trapping with high population can be achieved for cavities at a wide range of g .

C. Decoherence suppression in transient dynamics

The decoherence suppression and population trapping at EPs require optimizing the decay of one of eigenenergies in the system, and thus neglect the effects of EPs on the coherent QE-cavity interaction in the transient dynamics. In the following, we investigate the impact of EPs on the coherent energy exchange between the QE and the cavity, i.e., the Rabi oscillation.

Fig. 5(a) shows the time evolution of populations with initially excited QE resonant coupled to ES microcavity, where the Rabi oscillation is evident. The parameters are $g = 10\gamma$, $\kappa = 20\gamma$, and $\Delta\phi = \pi$. It shows that the maximum population of c_L cavity is slightly lower than the DP cavity, but it sustains for a longer time and four cycles of Rabi oscillation can be observed. While the Rabi oscillation of DP cavity manifests a faster decay, and the population of second-cycle oscillation is much smaller than that of ES microcavity. Meanwhile, the maximum population of c_R cavity is more than threefold compared to the DP cavity, and reaches ~ 0.66 . However, the period of Rabi oscillation is not obviously changed. The SE spectrum shown in the upper panel of Fig. 5(c) reveals that, it is because the splitting width is slightly enlarged, but the linewidth of Rabi peaks are greatly reduced. We highlight that the reduction of linewidth and the resultant slow decay of Rabi oscillation are attributed to the modification of LDOS by the EP term, see the inset of Fig. 5(a). In this sense, the decoherence suppression in ES microcavity is natural: EPs create a new kind of cavity with simultaneously narrower linewidth and larger LDOS than the usual DP cavity with Lorentzian response, and thus exhibits the superior property.

Fig. 5(b) shows the time evolution of populations for $g = 100\gamma$, where the decay of Rabi oscillation is slower than not only the DP cavity but also a bare QE. This is counterintuitive, since the coupling to a lossy cavity should increase the dissipation, and thus result in a faster decay. To gain insight into the problem, we obtain the approximate expressions of eigenenergies

$$\omega_{1,2} \approx \pm\sqrt{2}g + \frac{\kappa}{4} \sin(\Delta\phi) - i\frac{[\cos(\Delta\phi) + 1]\kappa + \gamma}{4} \quad (14)$$

$$\begin{aligned} \omega_3 \approx \frac{\kappa}{2} \sin(\Delta\phi) \left[\frac{\cos(\Delta\phi)}{C} - 1 \right] \\ - i\frac{\kappa}{2} \left[\cos(\Delta\phi) - 1 + \frac{\cos(2\Delta\phi)}{C} \right] \end{aligned} \quad (15)$$

where we expand the eigenenergies up to second order with respect to κ and γ . The white dashed lines in the lower panel of Fig. 5(d) track the energies of eigenenergy levels, and reveals that two eigenenergies of Eq. (14) correspond to the Rabi peaks in the SE spectrum

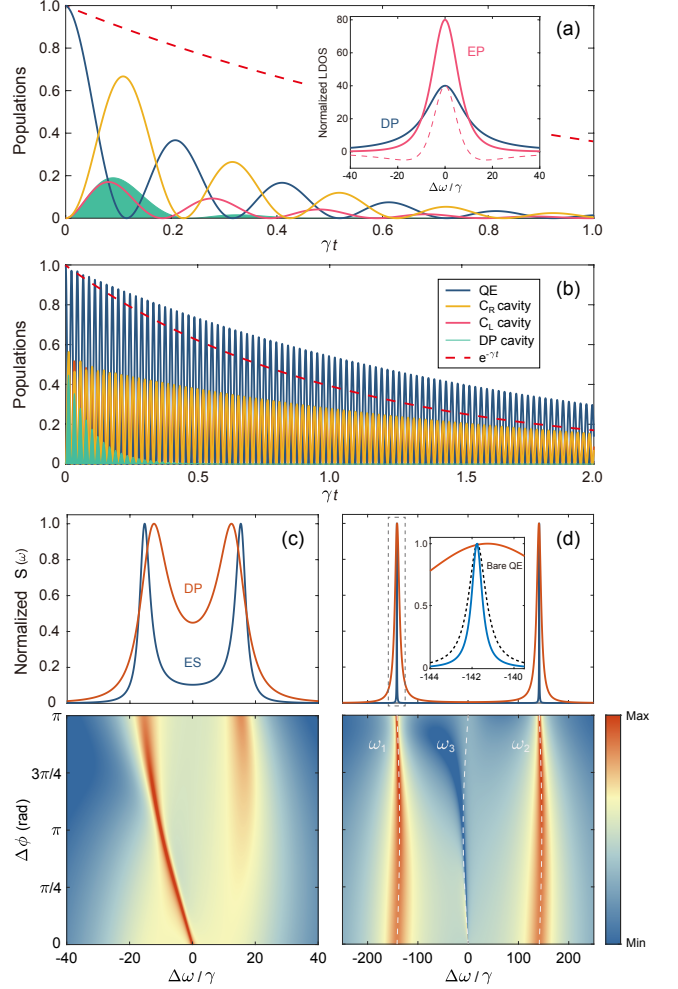


FIG. 5. Long-lasting Rabi oscillations in ES microcavity. (a) Population dynamics for QE (blue line), ES (yellow and pink lines) and DP (thin green line with shading) cavity modes. SE dynamics of a QE with the same decay rate is also shown for comparison (dashed red line). The parameters are $g = 10\gamma$, $\kappa = 20\gamma$, $\Delta_{0c} = 0$ and $\Delta\phi = \pi/2$. The inset plots the corresponding normalized LDOS. (b) is the same as (a) but for $g = 100\gamma$. The upper panels of (c) and (d) plot the normalized SE spectra corresponding to (a) and (b) for ES (blue lines) and DP (red lines) cavities, respectively. While the lower panels show the SE spectra versus $\Delta\phi$. The inset in the upper panel shows the Rabi peak with lower energy, where the SE spectrum of a bare QE is also presented for comparison (black dashed line). The white dashed lines in the lower panel track the energies of eigenenergy levels given by Eqs. (14) and (15).

shown in the upper panel of Fig. 5(d). Same as the case of $g = 10\gamma$, the SE spectrum exhibits the significant narrowing of Rabi peaks. However, Eq. (14) indicates that the linewidth narrowing in this case is anomalous, since the minimum decay achieved at $\Delta\phi = \pi$ is $-2 \text{Im}[\omega_{1,2}] \approx \gamma/2$, a half of a bare QE, see the inset in the upper panel of Fig. 5(d), where the SE spectrum of a bare QE is shown for comparison. Eq. (14) also indicates

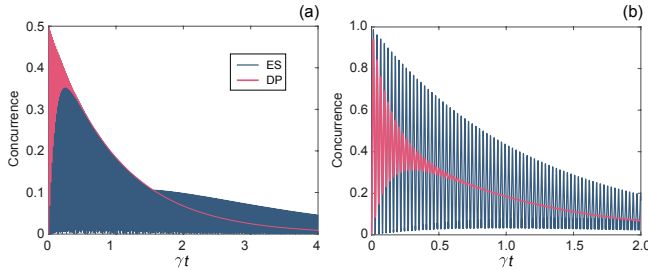


FIG. 6. Enhanced entanglement generation in ES microcavity. Dynamical concurrence between two qubits for $\Delta_{0c} = 2.32g$ (a) and $\Delta_{0c} = 0$ (b) in DP (red lines) and ES microcavity (blue lines). Other parameters are $g = 100\gamma$, $\kappa = 20\gamma$, and $\Delta\phi = \pi$. The results are numerically calculated using QuTip [80] with one qubit initially in the excited state while another in the ground state.

that the reduction of decay originates from the unidirectional coupling ($\kappa \cos(\Delta\phi)$ term) between two cavities for EPs, and thus unique to ES microcavity. The lower panels of Fig. 5(c) and (d) display the SE spectra as the function of $\Delta\phi$ for $g = 10\gamma$ and 100γ . It is interesting to see that though both are under the strong coupling regime with the equal splitting seen in SE spectrum at $\Delta\phi = \pi$, the underlying evolutions of two Rabi peaks are distinguishing. The Rabi peaks in the case of $g = 100\gamma$ are nearly unchanged as $\Delta\phi$ varies, while for $g = 10\gamma$, the Rabi peak with lower energy evolves from ω_c , and the linewidth is much narrower than the peak with higher energy until $\Delta\phi$ approaches to π .

The above results indicate that ES microcavity together with strong enough QE-cavity interaction will have significant advantages in quantum-optics applications, such as the spontaneous entanglement generation (SEG) between qubits. Extending our model into the multi-QE case is straightforward. Here we study the two-qubit SEG in ES microcavity, the generated entanglement is quantified by the concurrence $C(t)$ between qubits, which in our system is given by the simple expression $C(t) = 2|C_{eg}(t)C_{ge}^*(t)|$ [87], with $C_{eg}(t)$ and $C_{ge}(t)$ being the probability amplitudes of two single-excitation states that one qubit in the excited state while another in the ground state. We first consider the case of resonant qubit-cavity coupling, where the upper bound of maximum concurrence is 0.5. As shown in Fig. 6(a), the envelope of $C(t)$, exponentially decays with a rate of γ for a DP cavity, while in the ES microcavity, the evolution of $C(t)$ manifests two distinguishing stages with

different decay rates. The decay of envelope is identical as DP cavity before reaching the turning point, where an eigenstate with decay $\sim \kappa^3/32g^2$ starts to dominate the evolution of $C(t)$. With a large coupling rate $g = 100\gamma$, $\kappa^3/32g^2 = 1/40\gamma \ll \gamma$, and thus the decay of envelope at the second stage is much slower than a DP cavity. It also indicates that for a larger g , the decoherence suppression is more evident. Fig. 6(b) displays the dynamical concurrence corresponding to the maximum concurrence $C_{\max} = \max[C(t)] = 0.9866$, achieved with the optimal qubit-cavity detuning $\Delta_{0c} = 2.32g$. In this case, the envelope of $C(t)$ decay much faster in a DP cavity than the ES microcavity, which exhibits the great potential of ES microcavity to preserve the generated entanglement.

IV. CONCLUSION

In this work, we unravel some intriguing phenomena related to EPs in the cavity QED system based on a kind of WGM microcavity supporting an exceptional surface, and demonstrate the associated quantum-optics applications. An analytical description of LDOS and SE spectrum is presented to study the quantum effects of EPs, and understand the peculiar features of quantum dynamics at EPs. The results demonstrate the striking ability of EPs to suppress the decoherence occurred in the SE dynamics and the coherent light-matter interaction in the strong coupling regime, and thus we envision the EPs can offer the robustness again the dephasing for quantum devices, including but not limited to high-efficiency single-photon sources [88, 89], nonlinear interaction at the single-photon level [90], and high-fidelity entanglement generation and transport [91, 92]. Besides the nanophotonic structures, the quantum effects of EPs demonstrated in this work can also be implemented in other kind of platforms, such as superconducting [23, 93], cavity optomechanics [94, 95], and open cavity magnonic systems [24, 96]. We believe that our work can provide insight into the effects of EPs in a wide range of quantum systems and harnessing the non-Hermiticity for building novel quantum devices.

ACKNOWLEDGMENTS

We thank the support and the helpful discussion from Runhua Li, Yongyao Li, and Haishu Tan.

[1] C. M. Bender and S. Boettcher, Real spectra in non-hermitian hamiltonians having \mathcal{PT} symmetry, *Physical Review Letters* **80**, 5243 (1998).

[2] M.-A. Miri and A. Alù, Exceptional points in optics and photonics, *Science* **363**, eaar7709 (2019).

[3] S. K. Özdemir, S. Rotter, F. Nori, and L. Yang, Parity-time symmetry and exceptional points in photonics, *Nature Materials* **18**, 783 (2019).

[4] R. El-Ganainy, K. G. Makris, M. Khajavikhan, Z. H. Musslimani, S. Rotter, and D. N. Christodoulides, Non-hermitian physics and \mathcal{PT} symmetry, *Nature Physics* **14**,

11 (2018).

[5] E. J. Bergholtz, J. C. Budich, and F. K. Kunst, Exceptional topology of non-hermitian systems, *Reviews of Modern Physics* **93**, 015005 (2021).

[6] H. Hodaei, A. U. Hassan, S. Wittek, H. Garcia-Gracia, R. El-Ganainy, D. N. Christodoulides, and M. Khajavikhan, Enhanced sensitivity at higher-order exceptional points, *Nature* **548**, 187 (2017).

[7] W. Chen, S. Kaya Özdemir, G. Zhao, J. Wiersig, and L. Yang, Exceptional points enhance sensing in an optical microcavity, *Nature* **548**, 192 (2017).

[8] J. Wiersig, Enhancing the sensitivity of frequency and energy splitting detection by using exceptional points: Application to microcavity sensors for single-particle detection, *Physical Review Letters* **112**, 203901 (2014).

[9] Y.-H. Lai, Y.-K. Lu, M.-G. Suh, Z. Yuan, and K. Vahala, Observation of the exceptional-point-enhanced sagnac effect, *Nature* **576**, 65 (2019).

[10] M. P. Hokmabadi, A. Schumer, D. N. Christodoulides, and M. Khajavikhan, Non-hermitian ring laser gyroscopes with enhanced sagnac sensitivity, *Nature* **576**, 70 (2019).

[11] Q. Zhong, J. Ren, M. Khajavikhan, D. N. Christodoulides, S. K. Özdemir, and R. El-Ganainy, Sensing with exceptional surfaces in order to combine sensitivity with robustness, *Physical Review Letters* **122**, 153902 (2019).

[12] L. Feng, Z. J. Wong, R. M. Ma, Y. Wang, and X. Zhang, Single-mode laser by parity-time symmetry breaking, *Science* **346**, 972 (2014).

[13] H. Hodaei, M. A. Miri, M. Heinrich, D. N. Christodoulides, and M. Khajavikhan, Parity-time-symmetric microring lasers, *Science* **346**, 975 (2014).

[14] H. Xu, D. Mason, L. Jiang, and J. G. E. Harris, Topological energy transfer in an optomechanical system with exceptional points, *Nature* **537**, 80 (2016).

[15] J. Doppler, A. A. Mailybaev, J. Böhm, U. Kuhl, A. Girschik, F. Libisch, T. J. Milburn, P. Rabl, N. Moiseyev, and S. Rotter, Dynamically encircling an exceptional point for asymmetric mode switching, *Nature* **537**, 76 (2016).

[16] A. U. Hassan, B. Zhen, M. Soljačić, M. Khajavikhan, and D. N. Christodoulides, Dynamically encircling exceptional points: Exact evolution and polarization state conversion, *Physical Review Letters* **118**, 093002 (2017).

[17] H.-Z. Chen, T. Liu, H.-Y. Luan, R.-J. Liu, X.-Y. Wang, X.-F. Zhu, Y.-B. Li, Z.-M. Gu, S.-J. Liang, H. Gao, L. Lu, L. Ge, S. Zhang, J. Zhu, and R.-M. Ma, Revealing the missing dimension at an exceptional point, *Nature Physics* **16**, 571 (2020).

[18] Z. Lin, H. Ramezani, T. Eichelkraut, T. Kottos, H. Cao, and D. N. Christodoulides, Unidirectional invisibility induced by \mathcal{PT} -symmetric periodic structures, *Physical Review Letters* **106**, 213901 (2011).

[19] B. Peng, S. K. Özdemir, F. Lei, F. Monifi, M. Gianfreda, G. L. Long, S. Fan, F. Nori, C. M. Bender, and L. Yang, Parity-time-symmetric whispering-gallery microcavities, *Nature Physics* **10**, 394 (2014).

[20] M. Parto, Y. G. N. Liu, B. Bahari, M. Khajavikhan, and D. N. Christodoulides, Non-hermitian and topological photonics: optics at an exceptional point, *Nanophotonics* , 403 (2020).

[21] C. Wang, W. R. Sweeney, A. D. Stone, and L. Yang, Coherent perfect absorption at an exceptional point, *Science* **373**, 1261 (2021).

[22] H. Jiang, W. Zhang, G. Lu, L. Ye, H. Lin, J. Tang, Z. Xue, Z. Li, H. Xu, and Q. Gong, Exceptional points and enhanced nanoscale sensing with a plasmon-exciton hybrid system, *Photonics Research* **10**, 557 (2022).

[23] W. Chen, M. Abbasi, B. Ha, S. Erdamar, Y. N. Joglekar, and K. W. Murch, Decoherence-induced exceptional points in a dissipative superconducting qubit, *Physical Review Letters* **128**, 110402 (2022).

[24] X. Zhang, K. Ding, X. Zhou, J. Xu, and D. Jin, Experimental observation of an exceptional surface in synthetic dimensions with magnon polaritons, *Physical Review Letters* **123**, 237202 (2019).

[25] D. Zhang, X.-Q. Luo, Y.-P. Wang, T.-F. Li, and J. Q. You, Observation of the exceptional point in cavity magnon-polaritons, *Nature Communications* **8**, 1368 (2017).

[26] J. Zhao, Y. Liu, L. Wu, C.-K. Duan, Y.-x. Liu, and J. Du, Observation of anti-pt-symmetry phase transition in the magnon-cavity-magnon coupled system, *Physical Review Applied* **13**, 014053 (2020).

[27] W. Tang, X. Jiang, K. Ding, Y.-X. Xiao, Z.-Q. Zhang, C. T. Chan, and G. Ma, Exceptional nexus with a hybrid topological invariant, *Science* **370**, 1077 (2020).

[28] A. K. Jahromi, A. U. Hassan, D. N. Christodoulides, and A. F. Abouraddy, Statistical parity-time-symmetric lasing in an optical fibre network, *Nature Communications* **8**, 1359 (2017).

[29] S. Assawaworrarit, X. Yu, and S. Fan, Robust wireless power transfer using a nonlinear parity-time-symmetric circuit, *Nature* **546**, 387 (2017).

[30] Y. Li, Y.-G. Peng, L. Han, M.-A. Miri, W. Li, M. Xiao, X.-F. Zhu, J. Zhao, A. Alù, S. Fan, and C.-W. Qiu, Anti-parity-time symmetry in diffusive systems, *Science* **364**, 170 (2019).

[31] Y. Wu, W. Liu, J. Geng, X. Song, X. Ye, C. K. Duan, X. Rong, and J. Du, Observation of parity-time symmetry breaking in a single-spin system, *Science* **364**, 878 (2019).

[32] F. Klauck, L. Teuber, M. Ornigotti, M. Heinrich, S. Scheel, and A. Szameit, Observation of pt-symmetric quantum interference, *Nature Photonics* **13**, 883 (2019).

[33] R. Huang, S. K. Özdemir, J.-Q. Liao, F. Minganti, L.-M. Kuang, F. Nori, and H. Jing, Exceptional photon blockade, *arXiv* , 2001.09492 (2020).

[34] M. Naghiloo, M. Abbasi, Y. N. Joglekar, and K. W. Murch, Quantum state tomography across the exceptional point in a single dissipative qubit, *Nature Physics* **15**, 1232 (2019).

[35] Y. Choi, S. Kang, S. Lim, W. Kim, J. R. Kim, J. H. Lee, and K. An, Quasieigenstate coalescence in an atom-cavity quantum composite, *Physical Review Letters* **104**, 153601 (2010).

[36] H. Lü, S. Özdemir, L. M. Kuang, F. Nori, and H. Jing, Exceptional points in random-defect phonon lasers, *Physical Review Applied* **8**, 044020 (2017).

[37] J. Zhang, B. Peng, S. K. Özdemir, K. Pichler, D. O. Krimer, G. Zhao, F. Nori, Y.-x. Liu, S. Rotter, and L. Yang, A phonon laser operating at an exceptional point, *Nature Photonics* **12**, 479 (2018).

[38] S. Garmon, G. Ordóñez, and N. Hatano, Anomalous-order exceptional point and non-markovian purcell effect at threshold in one-dimensional continuum systems, *Physical Review Research* **3**, 033029 (2021).

[39] A. Purkayastha, M. Kulkarni, and Y. N. Joglekar, Emergent \mathcal{PT} symmetry in a double-quantum-dot circuit qed setup, *Physical Review Research* **2**, 043075 (2020).

[40] A. Pick, B. Zhen, O. D. Miller, C. W. Hsu, F. Hernandez, A. W. Rodriguez, M. Soljacic, and S. G. Johnson, General theory of spontaneous emission near exceptional points, *Optics Express* **25**, 12325 (2017).

[41] M. Khanbekyan and J. Wiersig, Decay suppression of spontaneous emission of a single emitter in a high- q cavity at exceptional points, *Physical Review Research* **2**, 023375 (2020).

[42] Q. Zhong, A. Hashemi, S. K. Özdemir, and R. El-Ganainy, Control of spontaneous emission dynamics in microcavities with chiral exceptional surfaces, *Physical Review Research* **3**, 013220 (2021).

[43] M. Zhang, W. Sweeney, C. W. Hsu, L. Yang, A. Stone, and L. Jiang, Quantum noise theory of exceptional point amplifying sensors, *Physical Review Letters* **123**, 180501 (2019).

[44] Y. Chu, Y. Liu, H. Liu, and J. Cai, Quantum sensing with a single-qubit pseudo-hermitian system, *Physical Review Letters* **124**, 020501 (2020).

[45] Z. Lin, A. Pick, M. Lončar, and A. W. Rodriguez, Enhanced spontaneous emission at third-order dirac exceptional points in inverse-designed photonic crystals, *Physical Review Letters* **117**, 107402 (2016).

[46] Y.-K. Lu, P. Peng, Q.-T. Cao, D. Xu, J. Wiersig, Q. Gong, and Y.-F. Xiao, Spontaneous t-symmetry breaking and exceptional points in cavity quantum electrodynamics systems, *Science Bulletin* **63**, 1096 (2018).

[47] J. Ren, S. Franke, and S. Hughes, Quasinormal mode theory of chiral power flow from linearly polarized dipole emitters coupled to index-modulated microring resonators close to an exceptional point, *ACS Photonics* **10**, 1021/acsphotonics.1c01848 (2022).

[48] M. Pelton, Modified spontaneous emission in nanophotonic structures, *Nature Photonics* **9**, 427 (2015).

[49] L. Novotny and B. Hecht, *Principles of nano-optics*, 2nd ed. (Cambridge University Press, 2012).

[50] G. Chen, Y.-C. Yu, X.-L. Zhuo, Y.-G. Huang, H. Jiang, J.-F. Liu, C.-J. Jin, and X.-H. Wang, Ab initio determination of local coupling interaction in arbitrary nanostructures: Application to photonic crystal slabs and cavities, *Physical Review B* **87**, 195138 (2013).

[51] J.-F. Liu, H.-X. Jiang, C.-J. Jin, X.-H. Wang, Z.-S. Gan, B.-H. Jia, and M. Gu, Orientation-dependent local density of states in three-dimensional photonic crystals, *Physical Review A* **85**, 015802 (2012).

[52] J. B. Khurgin and G. Sun, Comparative analysis of spasers, vertical-cavity surface-emitting lasers and surface-plasmon-emitting diodes, *Nature Photonics* **8**, 468 (2014).

[53] E. C. Andre, I. E. Protsenko, A. V. Uskov, J. Mork, and M. Wubs, On collective rabi splitting in nanolasers and nano-leds, *Optics Letters* **44**, 1415 (2019).

[54] A. Lenert, D. M. Bierman, Y. Nam, W. R. Chan, I. Celanović, M. Soljačić, and E. N. Wang, A nanophotonic solar thermophotovoltaic device, *Nature Nanotechnology* **9**, 126 (2014).

[55] S. I. Bozhevolnyi and J. B. Khurgin, Fundamental limitations in spontaneous emission rate of single-photon sources, *Optica* **3**, 10.1364/optica.3.001418 (2016).

[56] J. Liu, R. Su, Y. Wei, B. Yao, S. F. C. d. Silva, Y. Yu, J. Iles-Smith, K. Srinivasan, A. Rastelli, J. Li, and X. Wang, A solid-state source of strongly entangled photon pairs with high brightness and indistinguishability, *Nature Nanotechnology* **14**, 586 (2019).

[57] F. Liu, A. J. Brash, J. O'Hara, L. M. P. P. Martins, C. L. Phillips, R. J. Coles, B. Royall, E. Clarke, C. Bentham, N. Prtljaga, I. E. Itskevich, L. R. Wilson, M. S. Skolnick, and A. M. Fox, High purcell factor generation of indistinguishable on-chip single photons, *Nature Nanotechnology* **13**, 835 (2018).

[58] I. Söllner, S. Mahmoodian, S. L. Hansen, L. Midolo, A. Javadi, G. Kiršanské, T. Pagnolato, H. El-Ella, E. H. Lee, J. D. Song, S. Stobbe, and P. Lodahl, Deterministic photon-emitter coupling in chiral photonic circuits, *Nature Nanotechnology* **10**, 775 (2015).

[59] P. Lodahl, S. Mahmoodian, S. Stobbe, A. Rauschenbeutel, P. Schneeweiss, J. Volz, H. Pichler, and P. Zoller, Chiral quantum optics, *Nature* **541**, 473 (2017).

[60] W. D. Heiss, Green's functions at exceptional points, *International Journal of Theoretical Physics* **54**, 3954 (2015).

[61] J. Wiersig, Review of exceptional point-based sensors, *Photonics Research* **8**, 1457 (2020).

[62] B. Peng, S. K. Özdemir, M. Liertzer, W. Chen, J. Kramer, H. Yilmaz, J. Wiersig, S. Rotter, and L. Yang, Chiral modes and directional lasing at exceptional points, *Proceedings of the National Academy of Sciences USA* **113**, 6845 (2016).

[63] A. Hashemi, S. M. Rezaei, S. K. Özdemir, and R. El-Ganainy, New perspective on chiral exceptional points with application to discrete photonics, *APL Photonics* **6**, 040803 (2021).

[64] Y. Shen and J.-T. Shen, Nanoparticle sensing using whispering-gallery-mode resonators: Plasmonic and rayleigh scatterers, *Physical Review A* **85**, 013801 (2012).

[65] C. W. Gardiner, Driving a quantum system with the output field from another driven quantum system, *Physical Review Letters* **70**, 2269 (1993).

[66] H. J. Carmichael, Quantum trajectory theory for cascaded open systems, *Physical Review Letters* **70**, 2273 (1993).

[67] J.-T. Shen and S. Fan, Theory of single-photon transport in a single-mode waveguide. i. coupling to a cavity containing a two-level atom, *Physical Review A* **79**, 023837 (2009).

[68] J.-T. Shen and S. Fan, Theory of single-photon transport in a single-mode waveguide. ii. coupling to a whispering-gallery resonator containing a two-level atom, *Physical Review A* **79**, 023838 (2009).

[69] H. Pichler, T. Ramos, A. J. Daley, and P. Zoller, Quantum optics of chiral spin networks, *Physical Review A* **91**, 042116 (2015).

[70] C. A. Downing, J. C. L. Carreno, F. P. Laussy, E. del Valle, and A. I. Fernandez-Dominguez, Quasichiral interactions between quantum emitters at the nanoscale, *Physical Review Letters* **122**, 057401 (2019).

[71] K. Srinivasan and O. Painter, Mode coupling and cavity-quantum-dot interactions in a fiber-coupled microdisk cavity, *Physical Review A* **75**, 023814 (2007).

[72] J. Yang, S. Shi, X. Xie, S. Wu, S. Xiao, F. Song, J. Dang, S. Sun, L. Yang, Y. Wang, Z.-Y. Ge, B.-B. Li, Z. Zuo, K. Jin, and X. Xu, Enhanced emission from a single quantum dot in a microdisk at a deterministic diabolical point, *Optics Express* **29**, 14231 (2021).

[73] M. O. Scully and M. S. Zubairy, *Quantum optics* (Cambridge University Press, 1999).

[74] H. M. Doeleman, E. Verhagen, and A. F. Koenderink, Antenna-cavity hybrids: Matching polar opposites for purcell enhancements at any linewidth, *ACS Photonics* **3**, 1943 (2016).

[75] I. Medina, F. J. García-Vidal, A. I. Fernández-Domínguez, and J. Feist, Few-mode field quantization of arbitrary electromagnetic spectral densities, *Physical Review Letters* **126**, 093601 (2021).

[76] S. Franke, S. Hughes, M. K. Dezfouli, P. T. Kristensen, K. Busch, A. Knorr, and M. Richter, Quantization of quasinormal modes for open cavities and plasmonic cavity quantum electrodynamics, *Physical Review Letters* **122**, 213901 (2019).

[77] Y.-W. Lu, J.-F. Liu, Z. Liao, and X.-H. Wang, Plasmonic photonic cavity for high-efficiency single-photon blockade, *Science China Physics, Mechanics & Astronomy* **64**, 274212 (2021).

[78] C. Van Vlack, P. T. Kristensen, and S. Hughes, Spontaneous emission spectra and quantum light-matter interactions from a strongly coupled quantum dot metal-nanoparticle system, *Physical Review B* **85**, 025303 (2012).

[79] Y.-W. Lu, J.-F. Liu, R. Liu, R. Su, and X.-H. Wang, Quantum exceptional chamber induced by large nondipole effect of a quantum dot coupled to a nanoplasmonic resonator, *Nanophotonics* **10**, 2431 (2021).

[80] J. R. Johansson, P. D. Nation, and F. Nori, Qutip 2: A python framework for the dynamics of open quantum systems, *Computer Physics Communications* **184**, 1234 (2013).

[81] A. Imamoğlu, H. Schmidt, G. Woods, and M. Deutsch, Strongly interacting photons in a nonlinear cavity, *Physical Review Letters* **79**, 1467 (1997).

[82] E. Zubizarreta Casalengua, J. C. López Carreño, F. P. Laussy, and E. d. Valle, Conventional and unconventional photon statistics, *Laser & Photonics Reviews* **14**, 1900279 (2020).

[83] R. Liu, Z. K. Zhou, Y. C. Yu, T. Zhang, H. Wang, G. Liu, Y. Wei, H. Chen, and X. H. Wang, Strong light-matter interactions in single open plasmonic nanocavities at the quantum optics limit, *Physical Review Letters* **118**, 237401 (2017).

[84] C. W. Hsu, B. Zhen, A. D. Stone, J. D. Joannopoulos, and M. Soljačić, Bound states in the continuum, *Nature Reviews Materials* **1**, 16048 (2016).

[85] M. Cotrufo and A. Alù, Excitation of single-photon embedded eigenstates in coupled cavity-atom systems, *Optica* **6**, 799 (2019).

[86] H. Friedrich and D. Wintgen, Interfering resonances and bound states in the continuum, *Physical Review A* **32**, 3231 (1985).

[87] W. K. Wootters, Entanglement of formation of an arbitrary state of two qubits, *Physical Review Letters* **80**, 2245 (1998).

[88] H. Wang, Y.-M. He, T. H. Chung, H. Hu, Y. Yu, S. Chen, X. Ding, M. C. Chen, J. Qin, X. Yang, R.-Z. Liu, Z. C. Duan, J. P. Li, S. Gerhardt, K. Winkler, J. Jurkat, L.-J. Wang, N. Gregersen, Y.-H. Huo, Q. Dai, S. Yu, S. Höfling, C.-Y. Lu, and J.-W. Pan, Towards optimal single-photon sources from polarized microcavities, *Nature Photonics* **13**, 770 (2019).

[89] J. Iles-Smith, D. P. S. McCutcheon, A. Nazir, and J. Mørk, Phonon scattering inhibits simultaneous near-unity efficiency and indistinguishability in semiconductor single-photon sources, *Nature Photonics* **11**, 521 (2017).

[90] H. Choi, M. Heuck, and D. Englund, Self-similar nanocavity design with ultrasmall mode volume for single-photon nonlinearities, *Physical Review Letters* **118**, 223605 (2017).

[91] W.-K. Mok, D. Aghamalyan, J.-B. You, T. Haug, W. Zhang, C. E. Png, and L.-C. Kwek, Long-distance dissipation-assisted transport of entangled states via a chiral waveguide, *Physical Review Research* **2**, 013369 (2020).

[92] C. Gonzalez-Ballester, A. Gonzalez-Tudela, F. J. Garcia-Vidal, and E. Moreno, Chiral route to spontaneous entanglement generation, *Physical Review B* **92**, 155304 (2015).

[93] W. Nie, Z. Peng, F. Nori, and Y.-x. Liu, Topologically protected quantum coherence in a superatom, *Physical Review Letters* **124**, 10.1103/PhysRevLett.124.023603 (2020).

[94] I. Iorsh, A. Poshakinskiy, and A. Poddubny, Waveguide quantum optomechanics: Parity-time phase transitions in ultrastrong coupling regime, *Physical Review Letters* **125**, 183601 (2020).

[95] A. G. Primo, N. C. Carvalho, C. M. Kersul, N. C. Frateschi, G. S. Wiederhecker, and T. P. Alegre, Quasinormal-mode perturbation theory for dissipative and dispersive optomechanics, *Physical Review Letters* **125**, 233601 (2020).

[96] Y. P. Wang, J. W. Rao, Y. Yang, P. C. Xu, Y. S. Gui, B. M. Yao, J. Q. You, and C. M. Hu, Nonreciprocity and unidirectional invisibility in cavity magnonics, *Physical Review Letters* **123**, 127202 (2019).